

Limit Cycles and Chaos Induced by a Nonlinearity with Memory

K. J. H. Peters^{1,*} and S. R. K. Rodriguez^{1,†}

¹*Center for Nanophotonics, AMOLF, Science Park 104, 1098 XG Amsterdam, The Netherlands*
(Dated: August 6, 2021)

Inspired by the observation of a distributed time delay in the nonlinear response of an optical resonator, we investigate the effects of a similar delay on a noise-driven mechanical oscillator. For a delay time that is commensurate with the inverse dissipation rate, we find stable limit cycles. For longer delays, we discover a regime of chaotic dynamics associated with a double scroll attractor. We also analyze the effects of time delay on the spectrum and oscillation amplitude of the oscillator. Our results point to new opportunities for nonlinear energy harvesting, provided that a nonlinearity with distributed time delay can be implemented in mechanical systems.

Despite what Newton’s laws suggest, physical systems do not respond instantaneously. Real systems generally have a non-instantaneous response, which can be mathematically described by a time-delayed term in the equation of motion representing them [1–8]. Already a simple constant time delay can result in complex behavior, such as delay-induced bifurcations [9–11] and chaos [12, 13]. The more general classes of distributed time delays [14–18], time-varying delays [19–23] and state-dependent delays [24, 25] can also lead to a rich phenomenology. Beyond their fundamental relevance, time-delayed systems are also relevant to many applications in computation and machine learning [26–32], sensing [33–35], and chaos-based communication [36–38]. While a number of systems with nonlinear time delay have garnered strong interest [22, 39–42], most efforts in the field have focused on systems with time delay in their linear response.

Thermo-optical nonlinear cavities offer a convenient platform for probing an interesting type of nonlinear *distributed* time delay [43–46]. Optical experiments revealed that a nonlinearity with distributed time delay leads to a universal scaling law for hysteresis phenomena [45], and an enlarged bandwidth for noise-assisted amplification of periodic signals [46]. Motivated by these recent findings of fundamental and practical relevance, here we explore the physics of a noise-driven oscillator with variable distributed time delay in its nonlinear response. We demonstrate the emergence of stable limit cycles when the delay time is commensurate with the inverse dissipation rate of the oscillator. For larger delay times, we discover a chaotic regime associated with a double scroll attractor. Our results have implications for nonlinear vibration energy harvesters [47], which can be improved by a nonlinear response with distributed time delay.

Let us first demonstrate, experimentally, the existence of a distributed time delay in the thermo-optical nonlinear response of an oil-filled optical microcavity. Figure 1(a) illustrates our experimental setup: a tunable Fabry-Pérot cavity filled with macadamia oil and driven by a 532 nm continuous wave laser. The cavity [Fig. 1(b) inset] is made by a planar and a concave mirror. The planar mirror comprises a 60 nm silver layer on a glass substrate. The concave mirror has a diameter of 7 μm and a radius of curvature of 12 μm . It is fabricated by milling a glass substrate with a focused ion beam [48], and then coating it with a distributed Bragg reflector (DBR). The DBR has a peak reflectance of 99.9% at the center of the stopband, located at 530 nm. Thanks to micron-scale dimensions of the concave mirror strongly confining the optical modes, we can probe a single mode when scanning the cavity length across a wide (> 10 nm) range.

In a frame rotating at the frequency of the driving laser ω , the light field α in our cavity satisfies:

$$i\dot{\alpha}(t) = \left[-\Delta - i\frac{\Gamma}{2} + U \int_0^t ds K(t-s) (|\alpha(s)|^2 - 1) \right] \alpha(t) + i\sqrt{\kappa_L}F + \frac{D}{\sqrt{2}} [\xi_1(t) + i\xi_2(t)]. \quad (1)$$

$\Delta = \omega - \omega_0$ is the laser-cavity detuning, with ω_0 the cavity resonance frequency. $\Gamma = \gamma + \kappa_L + \kappa_R$ is the total dissipation rate, with γ the intrinsic loss rate, and κ_L (κ_R) the input-output coupling rate through the left (right) mirror. U quantifies the strength of the cubic nonlinearity, corresponding to effective photon-photon interactions in optical systems. The memory kernel $K(t) = \exp(-t/\tau)/\tau$ accounts for the non-instantaneous nonlinear response of our cavity, i.e., the distributed time delay. This time-delayed response arises because the temperature of the oil takes a finite time to relax to a steady state when the laser amplitude F changes. The term $D\xi(t) = D[\xi_1(t) + i\xi_2(t)]/\sqrt{2}$ represents Gaussian white noise with variance D^2 in the laser amplitude and phase. $\xi_i(t)$ each have zero mean [i.e., $\langle \xi_i(t) \rangle = 0$], and are delta-correlated with unit variance [i.e., $\langle \xi_i(t)\xi_i(t+t') \rangle = \delta(t')$]. Moreover, $\xi_1(t)$ and $\xi_2(t)$ are mutually uncorrelated. We numerically solve Eq. 1 (and equations ahead) using the xSPDE toolbox [49] for Matlab.

For strong driving (large F), the cavity supports optical bistability: two stable steady states with different intra-cavity intensity $|\alpha|^2$ at a single driving condition. To evidence bistability, we measure the transmitted intensity while

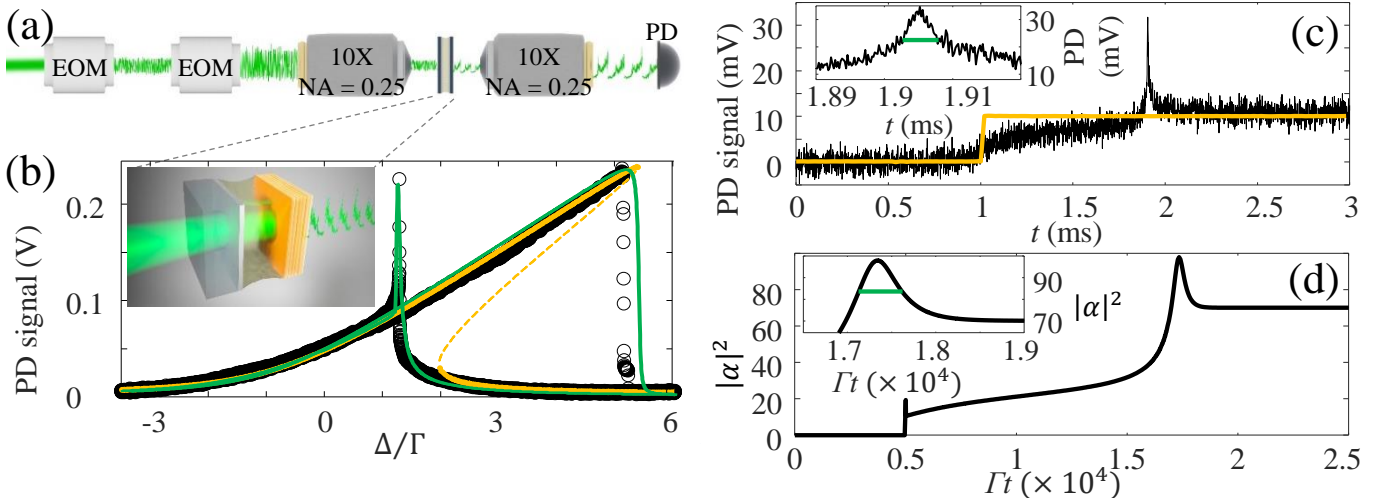


FIG. 1. (a) Schematic of our optical setup. Two electro-optical modulators (EOM) add noise to the laser amplitude and phase. The laser light is then focused on an oil-filled optical microcavity using microscope objectives. The transmitted light is measured using a photodetector (PD). (b) Transmitted intensity while opening and closing the cavity (black circles), averaged over 20 cycles. Yellow solid (dashed) curves show stable (unstable) steady-state solutions of Eq. 1. Green solid curve shows a dynamical simulation while scanning Δ/Γ . Inset: Schematic of an oil-filled optical microcavity. (c) Transmitted intensity (black) when the input laser is modulated by a chopper, creating a step function in the intensity (yellow). Inset: Zoom of overshoot. Green line indicates the full-width half-maximum of the overshoot, which is $5 \mu\text{s}$. (d) Simulation of Eq. 1 when increasing F from 0 to $7\sqrt{\Gamma}$ at $\Gamma t = 5000$. Inset: Zoom of the overshoot. Green line indicates width of the overshoot, which is $\tau/2$.

scanning the cavity length (and hence Δ) forward and backward. The black curve in Fig. 1(b) shows the result when the laser power is 7.8 mW at the excitation objective. We observe a large optical hysteresis, and bistability occurs in the $1.5 \lesssim \Delta/\Gamma \lesssim 5$ range. We also observe a large overshoot around $\Delta/\Gamma = 1.5$, which is due to the non-instantaneous thermo-optical nonlinearity of the oil-filled cavity. The solid (dashed) yellow curve in Fig. 1(b) shows stable (unstable) steady-state solutions, obtained by setting $\dot{\alpha} = 0$ in Eq. 1. These steady-state calculations reproduce the bistability, but not the overshoot. In contrast, dynamical simulations of Eq. 1, shown as solid green curves in Fig. 1(b), reproduce our experimental observations including the overshoot. The overshoot arises when the duration of the scan is similar to or less than the thermal relaxation time of the oil [45], which is the case in our experiments.

Figures 1(c,d) further evidence the non-instantaneous nonlinear response of our cavity. The black curve in Fig. 1(c) represents the transmitted intensity when modulating the laser power in a step-like fashion, as shown by the yellow curve. Prior to the step, the laser is blocked and the transmission is zero. Immediately after the step, the transmission first increases to a low intensity state. Then, the nonlinearity gradually builds up due to the laser-induced heating of the oil. This results in a slow increase of the transmitted signal. Finally, after the nonlinearity has sufficiently built up, the transmitted intensity displays a large overshoot followed by relaxation to a high intensity steady state. In Fig. 1(d) we numerically reproduce our experimental observations using Eq. 1. From our calculations we find that the full-width at half-maximum of the overshoot, indicated by the green line in the Fig. 1(c) inset, is $\tau/2$ regardless of the cavity parameters. Based on this finding, we deduce that the nonlinearity of our oil-filled cavity has a distributed time delay with $\tau = 10 \mu\text{s}$.

The results in Fig. 1 and in References [45, 46] motivate us to explore more generally, beyond the realm of optics, the effects of a nonlinearity with distributed time delay. In this spirit, we consider a mechanical oscillator with a Duffing-type nonlinearity having distributed time delay. We describe the time delay with the same kernel function $K(t)$ used to describe our oil-filled cavity. Thus, our nonlinear oscillator satisfies the following equation of motion:

$$m\ddot{x}(t) = \left(a + b \int_0^t ds K(t-s)x(s)^2 \right) x(t) - \gamma\dot{x}(t) + D\xi(t). \quad (2)$$

m is the mass of the oscillator and γ its dissipation. a and b define the potential $V(x) = -ax^2/2 + bx^4/4$ in the limit $\tau \rightarrow 0$. We set $a > 0$ and $b > 0$, such that $V(x)$ is a double-well potential.

To simulate Eq. 2 it is convenient to define the variables $w = b \int_0^t ds K(t-s)x(s)^2$ and $v = \dot{x}$. This allows us to

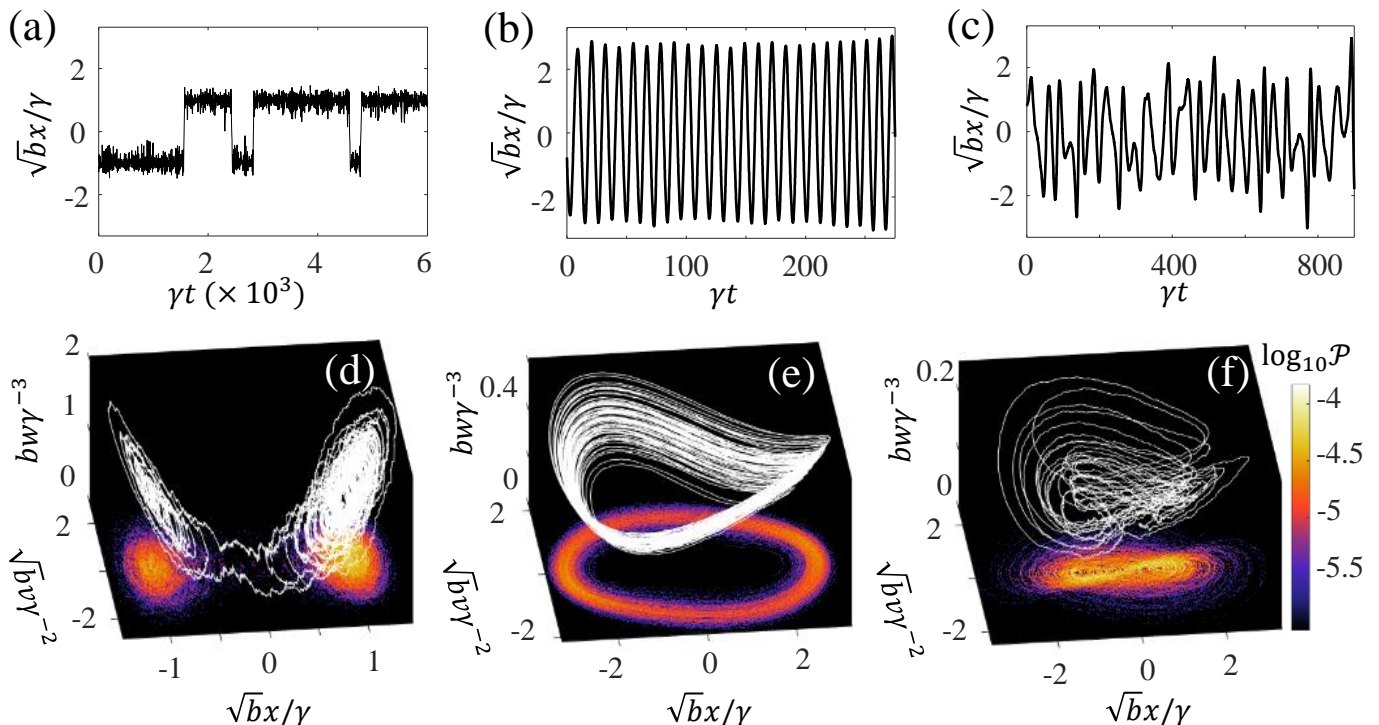


FIG. 2. Simulations of an oscillator with Duffing-type nonlinearity having distributed time delay. γ is the dissipation rate and τ is the memory time. (a)-(c) show position as function of time for $\gamma\tau = 10^{-2}$, $\gamma\tau = 3$, and $\gamma\tau = 20$, respectively. (d)-(f) show the phase space trajectories for trajectories of duration $\gamma t = 10^3$. The color plot in the x, v plane is a 2D histogram built from a trajectory of duration $\gamma t = 10^4$. Simulation parameters: $\gamma = 1$, $a = 1$, $b = a/10$, $m = 10a\gamma^{-2}$, $D^2 = \gamma$.

write Eq. 2 as a set of 3 ordinary differential equations

$$\begin{aligned}
 \dot{x} &= v, \\
 m\dot{v} &= (a - w)x - \gamma v + D\xi(t), \\
 \dot{w} &= (bx^2 - w)/\tau,
 \end{aligned} \tag{3}$$

which we solve numerically using a fourth-order Runge-Kutta algorithm with time increments $\Delta t = \gamma^{-1}/100$.

The dynamics of our nonlinear oscillator strongly depend on the memory time τ . In Fig. 2(a) we plot a trajectory of x for $\gamma\tau \ll 1$, i.e., in the limit of an instantaneous nonlinear response. We observe random transitions between the two minima of $V(x)$, located at $x_{\pm} = \pm\sqrt{a/b}$. This is the typical behavior of a bistable system. Figure 2(d) shows the corresponding trajectory in phase space. The projection of that trajectory on the x, v plane shows the expected behavior for a noise-driven Duffing oscillator without memory. Figures 2(b) and 2(e) show a typical trajectory in time and phase space, respectively, when $\gamma\tau \gtrsim 1$. In that case, we observe stable limit cycles with an amplitude far exceeding the distance between the two minima of $V(x)$. The limit cycles arise due to a Hopf bifurcation near $\gamma\tau = 1$. Finally, for certain ranges of $\gamma\tau > 1$, the dynamics become chaotic. An example of this chaotic regime is shown in Figs. 2(c,f). Notice in Fig. 2(f) the characteristic shape of the double scroll attractor, indicative of chaos [50].

Figure 3(a) shows a bifurcation diagram for our mechanical oscillator as $\gamma\tau$ increases. We plot the x -values where the phase space trajectory crosses the manifold $v = 0$ with $\dot{v} > 0$. For $\gamma\tau < 13.6$ we observe a single point for each $\gamma\tau$, indicating a period-1 limit cycle [Fig. 3(b)]. Near $\gamma\tau = 13.6$ we observe a bifurcation, whereafter a period-2 limit cycle arises [Fig. 3(c)]. Finally, for $\gamma\tau > 16.5$ we observe the double scroll attractor characteristic of deterministic chaos. The figure as a whole (and the inset in more detail) shows the typical cascade of period-doubling bifurcations leading to chaos. Notice that we also observe periodic windows in between chaotic regimes, occurring within certain ranges of $\gamma\tau$.

Figure 4(a) shows the spectral response of the oscillator for different τ . The spectra are obtained by Fourier transforming the time traces in Fig. 2. For $\gamma\tau = 10^{-2}$, the orange curve shows a single shallow peak near the resonance frequency ω_{\pm} for the $\tau = 0$ case. The peak deviates slightly from $\omega_{\pm} = a/m$ because of the finite τ in our system. Moving on to $\gamma\tau = 3$, the black curve in Fig. 4(a) reveals a strong peak at $f/\gamma \approx 0.09$. This peak corresponds

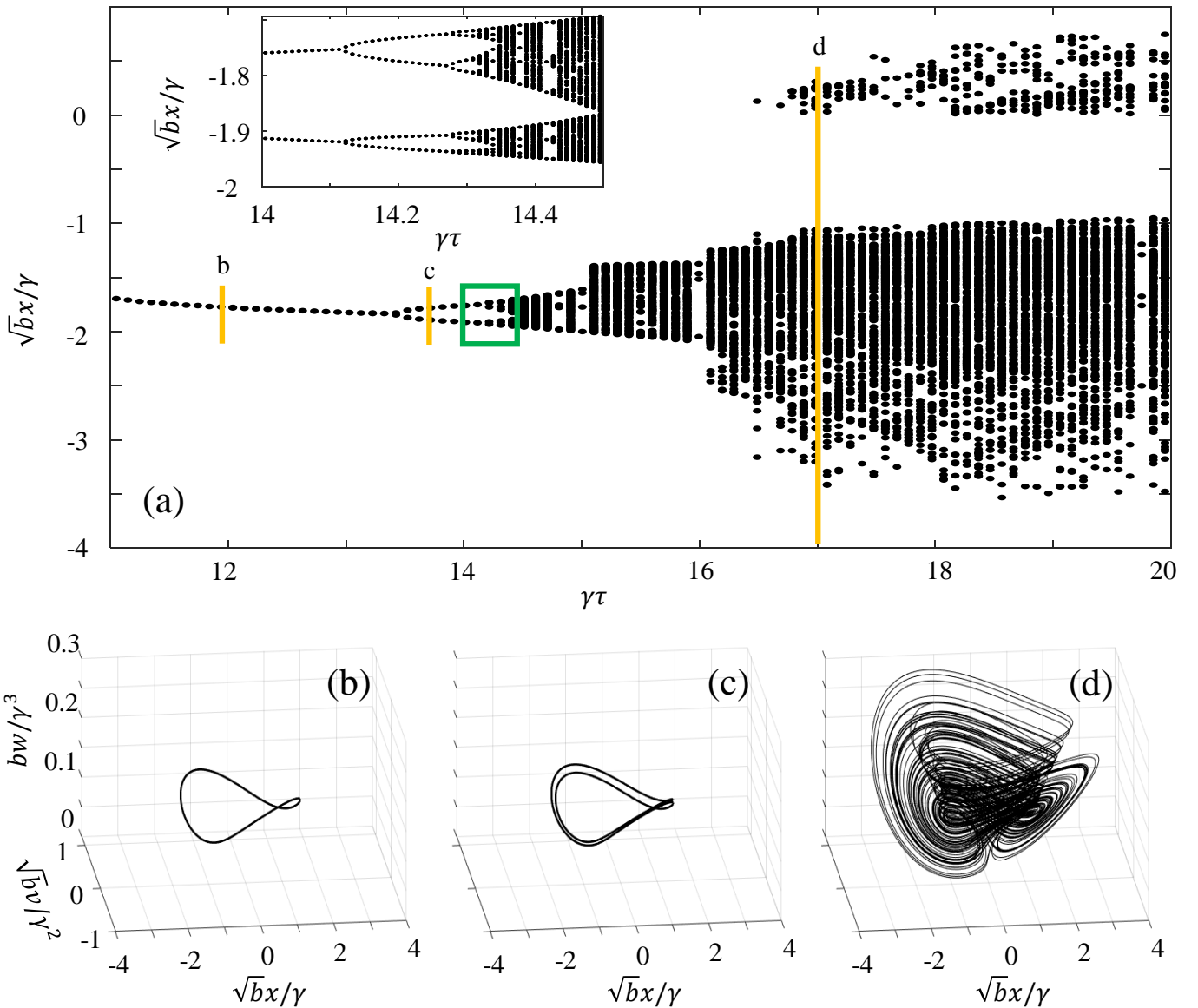


FIG. 3. (a) Bifurcation diagram as function of $\gamma\tau$. Vertical yellow lines indicate the phase space trajectories in (b)-(d). Inset: Zoom of region in the green rectangle. Parameters are as in Fig. 2 with $D = 0$.

to the large amplitude limit cycle oscillations observed in Fig. 2(b). We also notice a peak around $f/\gamma \approx 0.27$, due to the oscillations not being purely sinusoidal. Moving on to the chaotic regime ($\gamma\tau = 20$), the green curve in Fig. 4(a) no longer shows any well-resolved resonances. This is expected based on the fact that chaotic dynamics can involve a wide range of frequency components. Thinking about nonlinear energy harvesting applications [47], one could imagine that chaotic broadband dynamics may be advantageous, since one would like to extract noise power from a wide spectral range. However, Fig. 4(a) shows that the power spectrum for the chaotic oscillator decays significantly at high frequencies. Thus, to assess the frequency-integrated effect of the memory time, let us analyze the root-mean-square (RMS) displacement x_{rms} of the oscillator.

Figure 4(b) shows x_{rms} normalized to the average value in the small τ limit, $\langle x_{\text{rms}}^0 \rangle$, as function of $\gamma\tau$. We observe that $x_{\text{rms}}/\langle x_{\text{rms}}^0 \rangle \approx 1$ in the Markovian limit ($\gamma\tau \ll 1$), where memory effects are irrelevant. In contrast, the RMS displacement is greatly enhanced for $\gamma\tau \gtrsim 1$. As $\gamma\tau$ increases beyond 1, the RMS displacement decreases because of the chaotic dynamics. For $\gamma\tau \gg 1$ the RMS displacement remains constant as function of $\gamma\tau$, since the system is effectively linear in this regime. However, the RMS displacement is still larger than in the Markovian limit because the system can intermittently make large amplitude excursions and then relax to the monostable state again. Finally, we would like to point out that the lack of data points in the range $\gamma\tau = 0.2 - 3$ is due to lack of numerical convergence.

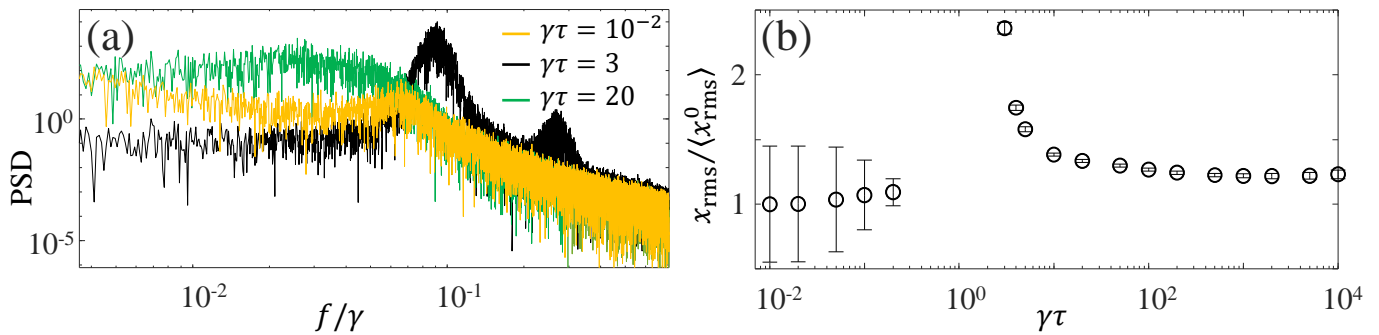


FIG. 4. (a) Power spectral density of an oscillator with Duffing-type nonlinearity having distributed time delay. γ is the dissipation rate and τ is the memory time. (b) Enhancement of the root-mean-squared displacement with respect to $\gamma\tau = 10^{-2}$ as function of $\gamma\tau$. Parameters are as in Fig. 2.

In our simulations, the amplitude of the limit cycle oscillations diverges in this range. While we believe that more sophisticated numerical methods may resolve this issue, limit cycle oscillations of very large amplitude are still likely to be found in that regime.

To summarize, we have demonstrated how a distributed time delay in a Duffing-type nonlinearity can lead to a rich phenomenology, including the emergence of stable limit cycles and chaos. Remarkably, the amplitude of the limit cycle oscillations can be very large when the delay time is commensurate with the dissipation time. If such a distributed time delay can be realized in nonlinear energy harvesters [47], our results could pave the way for massively improving the performance of those systems.

ACKNOWLEDGMENTS

This work is part of the research programme of the Netherlands Organisation for Scientific Research (NWO). We thank Carlos Pando Lambruschini and Panayotis Panayotaros for organizing the workshop on Advanced Computational and Experimental Techniques in Nonlinear Dynamics, which stimulated this manuscript. We also thank Jason Smith, Aurelien Trichet, and Kiana Malmir for providing the concave mirror used for the experiments in Figure 1. S.R.K.R. acknowledges an ERC Starting Grant with project number 85269.

* k.peters@amolf.nl

† s.rodriguez@amolf.nl

- [1] O.V. Popovych, S. Yanchuk, and P.A. Tass. Delay-and coupling-induced firing patterns in oscillatory neural loops. *Phys. Rev. Lett.*, 107(22):228102, 2011.
- [2] Y. Kuang. *Delay differential equations*. University of California Press, 2012.
- [3] J. Liu and Z. Zhang. Dynamics of a predator-prey system with stage structure and two delays. *J. Nonlinear Sci. Appl.*, 9(5):3074–3089, 2016.
- [4] X.-M. Zhang. Recent developments in time-delay systems and their applications, 2019.
- [5] A. Keane, B. Krauskopf, and C.M. Postlethwaite. Climate models with delay differential equations. *Chaos*, 27(11):114309, 2017.
- [6] S. Terrien, B. Krauskopf, N.G.R. Broderick, R. Braive, G. Beaudoin, I. Sagnes, and S. Barbay. Pulse train interaction and control in a microcavity laser with delayed optical feedback. *Opt. Lett.*, 43(13):3013–3016, Jul 2018.
- [7] A. Otto, W. Just, and G. Radons. Nonlinear dynamics of delay systems: An overview. *Philos. Trans. Royal Soc. A*, 377(2153):20180389, 2019.
- [8] J.D. Hart, . Larger, T.E. Murphy, and R. Roy. Delayed dynamical systems: Networks, chimeras and reservoir computing. *Philos. Trans. Royal Soc. A*, 377(2153):20180123, 2019.
- [9] J. Xu and P. Yu. Delay-induced bifurcations in a nonautonomous system with delayed velocity feedbacks. *Int. J. Bifurc. Chaos Appl. Sci. Eng.*, 14(08):2777–2798, 2004.
- [10] L.P. Shayer and S.A. Campbell. Stability, bifurcation, and multistability in a system of two coupled neurons with multiple time delays. *SIAM J. Appl. Math.*, 61(2):673–700, 2000.
- [11] X. Liao and G. Chen. Local stability, Hopf and resonant codimension-two bifurcation in a harmonic oscillator with two time delays. *Int. J. Bifurc. Chaos Appl. Sci. Eng.*, 11(08):2105–2121, 2001.

- [12] U. an der Heiden and H.-O. Walther. Existence of chaos in control systems with delayed feedback. *J. Differ. Equ.*, 47(2):273–295, 1983.
- [13] L.A. Safonov, E. Tomer, V.V. Strygin, Y. Ashkenazy, and S. Havlin. Delay-induced chaos with multifractal attractor in a traffic flow model. *Europhys. Lett.*, 57(2):151, 2002.
- [14] H. Wang, H. Hu, and Z. Wang. Global dynamics of a Duffing oscillator with delayed displacement feedback. *Int. J. Bifurc. Chaos Appl. Sci. Eng.*, 14(08):2753–2775, 2004.
- [15] Z. Sun, W. Xu, X. Yang, and T. Fang. Inducing or suppressing chaos in a double-well Duffing oscillator by time delay feedback. *Chaos Solitons Fractals*, 27(3):705–714, 2006.
- [16] C. Jeevarathinam, S. Rajasekar, and M.A.F. Sanjuán. Vibrational resonance in the Duffing oscillator with distributed time-delayed feedback. *J. Appl. Nonlinear Dyn.*, 4(4):391–404, 2015.
- [17] J. Cantisán, M. Coccolo, J.M. Seoane, and M.A.F. Sanjuán. Delay-induced resonance in the time-delayed Duffing oscillator. *Int. J. Bifurc. Chaos Appl. Sci. Eng.*, 30(03):2030007, 2020.
- [18] M. Coccolo, J. Cantisán, J.M. Seoane, S. Rajasekar, and M.A.F. Sanjuán. Delay-induced resonance suppresses damping-induced unpredictability. *Philos. Trans. Royal Soc. A*, 379(2192):20200232, 2021.
- [19] J. Louisell. Delay differential systems with time-varying delay: New directions for stability theory. *Kybernetika*, 37(3):239–251, 2001.
- [20] T. Botmart, P. Niamsup, and X. Liu. Synchronization of non-autonomous chaotic systems with time-varying delay via delayed feedback control. *Commun. Nonlinear Sci. Numer. Simul.*, 17(4):1894–1907, 2012.
- [21] A. Ardjouni and A. Djoudi. Existence of positive periodic solutions for a nonlinear neutral differential equation with variable delay. *Appl. Math. E-Notes*, 12:94–101, 2012.
- [22] D. Müller, A. Otto, and G. Radons. Laminar chaos. *Phys. Rev. Lett.*, 120(8):084102, 2018.
- [23] D. Müller-Bender, A. Otto, and G. Radons. Resonant Doppler effect in systems with variable delay. *Philos. Trans. Royal Soc. A*, 377(2153):20180119, 2019.
- [24] T. Insperger, G. Stépán, and J. Turi. State-dependent delay in regenerative turning processes. *Nonlinear Dyn.*, 47(1):275–283, 2007.
- [25] A. Keane, B. Krauskopf, and H.A. Dijkstra. The effect of state dependence in a delay differential equation model for the El Niño southern oscillation. *Philos. Trans. Royal Soc. A*, 377(2153):20180121, 2019.
- [26] S. Ortín, M.C. Soriano, L. Pesquera, D. Brunner, D. San-Martín, I. Fischer, C.R. Mirasso, and J.M. Gutiérrez. A unified framework for reservoir computing and extreme learning machines based on a single time-delayed neuron. *Sci. Rep.*, 5(1):1–11, 2015.
- [27] J.D. Hart, L. Larger, T.E. Murphy, and R. Roy. Delayed dynamical systems: Networks, chimeras and reservoir computing. *Philos. Trans. Royal Soc. A*, 377(2153):20180123, 2019.
- [28] B. Penkovsky, X. Porte, M. Jacquot, L. Larger, and D. Brunner. Coupled nonlinear delay systems as deep convolutional neural networks. *Phys. Rev. Lett.*, 123(5):054101, 2019.
- [29] V.A. Pammi, K. Alfaro-Bittner, M.G. Clerc, and S. Barbay. Photonic computing with single and coupled spiking micropillar lasers. *IEEE J. Sel. Top. Quantum Electron.*, 26(1):1–7, 2020.
- [30] K. Harkhoe, G. Verschaffelt, A. Katumba, P. Bienstman, and G. Van der Sande. Demonstrating delay-based reservoir computing using a compact photonic integrated chip. *Opt. Express*, 28(3):3086–3096, Feb 2020.
- [31] D. Brunner, L. Larger, and M.C. Soriano. Nonlinear photonic dynamical systems for unconventional computing. *arXiv preprint arXiv:2107.08874*, 2021.
- [32] A. Banerjee, J.D. Hart, R. Roy, and E. Ott. Machine learning link inference of noisy delay-coupled networks with optoelectronic experimental tests. *Phys. Rev. X*, 11(3):031014, 2021.
- [33] V.V. Grigor'yants, A.A. Dvornikov, Y.B. Il'in, V.N. Konstantinov, V.A. Prokof'iev, and G.M. Utkin. A laser diode with feedback using a fibre delay line as a stable-frequency signal generator and potential fibre sensor. *Opt. Quantum Electron.*, 17(4):263–267, 1985.
- [34] X. Zou, X. Liu, W. Li, P. Li, W. Pan, L. Yan, and L. Shao. Optoelectronic oscillators (oeos) to sensing, measurement, and detection. *IEEE J. Quantum Electron.*, 52(1):1–16, 2015.
- [35] J. Yao. Optoelectronic oscillators for high speed and high resolution optical sensing. *J. Light. Technol.*, 35(16):3489–3497, 2017.
- [36] L. Larger, J.-P. Goedgebuer, and V. Udaltsov. Ikeda-based nonlinear delayed dynamics for application to secure optical transmission systems using chaos. *C. R. Phys.*, 5(6):669–681, 2004.
- [37] C. Li, X. Liao, and K.-W. Wong. Chaotic lag synchronization of coupled time-delayed systems and its applications in secure communication. *Physica D*, 194(3-4):187–202, 2004.
- [38] N. Jiang, W. Pan, L. Yan, B. Luo, S. Xiang, L. Yang, D. Zheng, and N. Li. Chaos synchronization and communication in multiple time-delayed coupling semiconductor lasers driven by a third laser. *IEEE J. Sel. Top. Quantum Electron.*, 17(5):1220–1227, 2011.
- [39] M.C. Mackey and L. Glass. Oscillation and chaos in physiological control systems. *Science*, 197(4300):287–289, 1977.
- [40] K. Ikeda. Multiple-valued stationary state and its instability of the transmitted light by a ring cavity system. *Opt. Commun.*, 30(2):257–261, 1979.
- [41] S. Lepri, G. Giacomelli, A. Politi, and F.T. Arecchi. High-dimensional chaos in delayed dynamical systems. *Physica D*, 70(3):235–249, 1994.
- [42] J.D. Hart, R. Roy, D. Müller-Bender, A. Otto, and G. Radons. Laminar chaos in experiments: Nonlinear systems with time-varying delays and noise. *Phys. Rev. Lett.*, 123:154101, Oct 2019.

- [43] A.M. Yacomotti, P. Monnier, F. Raineri, B.B. Bakir, C. Seassal, R. Raj, and J.A. Levenson. Fast thermo-optical excitability in a two-dimensional photonic crystal. *Phys. Rev. Lett.*, 97:143904, Oct 2006.
- [44] H. Alaeian, M. Schedensack, C. Bartels, D. Peterseim, and M. Weitz. Thermo-optical interactions in a dye-microcavity photon Bose–Einstein condensate. *New J. Phys.*, 19(11):115009, nov 2017.
- [45] Z. Geng, K.J.H. Peters, A.A.P. Trichet, K. Malmir, R. Kolkowski, J.M. Smith, and S.R.K. Rodriguez. Universal scaling in the dynamic hysteresis, and non-Markovian dynamics, of a tunable optical cavity. *Phys. Rev. Lett.*, 124(15):153603, 2020.
- [46] K.J.H. Peters, Z. Geng, K. Malmir, J.M. Smith, and S.R.K. Rodriguez. Extremely broadband stochastic resonance of light and enhanced energy harvesting enabled by memory effects in the nonlinear response. *Phys. Rev. Lett.*, 126(21):213901, 2021.
- [47] F. Cottone, H. Vocca, and L. Gammaitoni. Nonlinear energy harvesting. *Phys. Rev. Lett.*, 102(8):080601, 2009.
- [48] A.A.P. Trichet, P.R. Dolan, D.M. Coles, G.M. Hughes, and J.M. Smith. Topographic control of open-access microcavities at the nanometer scale. *Opt. Express*, 23(13):17205–17216, Jun 2015.
- [49] S. Kieseewetter, R. Polkinghorne, B. Opanchuk, and P.D. Drummond. xSPDE: Extensible software for stochastic equations. *SoftwareX*, 5:12 – 15, 2016.
- [50] L. Chua, M. Komuro, and T. Matsumoto. The double scroll family. *IEEE Trans. Circuits Syst.*, 33(11):1072–1118, 1986.